Chemical Science

ROYAL SOCIETY OF CHEMISTRY

EDGE ARTICLE

View Article Online
View Journal

Cite this: DOI: 10.1039/d0sc00219d

All publication charges for this article have been paid for by the Royal Society of Chemistry

Received 13th January 2020
Accepted 27th January 2020

DOI: 10.1039/d0sc00219d

rsc.li/chemical-science

Synthesis of AB_n-type colloidal molecules by polymerization-induced particle-assembly (PIPA)†‡

Dan Li,§[a] Xi Chen,§[a] Min Zeng,[a] Jinzhao Ji,[a] Yun Wang,[a] Zhenzhong Yang *[b] and Jinying Yuan *[a]

Conventional synthesis of colloidal molecules (CMs) mainly depends on particle-based self-assembly of patchy building blocks. However, direct access to CMs by the self-assembly of isotropic colloidal subunits remains challenging. Here, we report the mass production of AB_n-type CMs by polymerization-induced particle-assembly (PIPA), using a linear ABC triblock terpolymer system. Starting from diblock copolymer spheres, the association of spheres takes place *in situ* during the polymerization of the third block. The third blocks aggregate into attractive domains, which connect spheres into CMs. The stability of CMs is ensured, as long as the conversions are limited to *ca.* 50%, and the pH is low. The valence of AB_n-type CMs ($n = 2–6$) is determined by the volume ratio of the polymer blocks. By tuning the volume ratio, 78.5% linear AB_2-type CMs are yielded. We demonstrate that polymerization-induced particle-assembly is successful for the scalable fabrication of AB_n-type CMs (50 g L^{-1}), and can be easily extended to vastly different triblock terpolymers, for a wide range of applications.

Introduction

Colloidal molecules (CMs) are well-defined colloidal clusters with precise symmetry of molecular structures and have drawn extensive interest because of their unique properties[1,2] and potential as building blocks for low-coordination open structures.[3,4] With compartmental functional domains and directional interaction, CMs are promising in biological and medical applications,[5,6] self-assembly,[7,8] physical chemistry,[9–11] and materials science and technology.[12–14] Through particle-based self-assembly, CMs with molecule-like symmetries are enabled using monodisperse patchy building blocks with a suitable shape or interaction anisotropy. There are continuing efforts to develop methods toward patchy building blocks,[15,16] including colloidal crystal templating,[17] seeded emulsion polymerization,[18] assembly of oppositely charged particles,[19–21] DNA origami,[22–24] self-assembly of block copolymers,[25–28] and emulsion solvent-evaporation methods.[29–31] However, these methods struggle in fabricating controllable patches with desired size (10–100 nm). In this size regime, the synthesis of monodisperse building block is difficult, and irregularity causes defects which amplify throughout the hierarchical self-assembly. Therefore, efficient access to CMs remains challenging.

Over the past few years, self-assembly of block copolymers (BCPs) has emerged as an elegant bottom-up technique to produce soft nanoparticles with controllable structures, sizes, and functions.[32–34] The polymerization-induced self-assembly (PISA) technique has experienced great success in the mass production of self-assembled BCPs, where the synthesis and self-assembly of BCPs are achieved simultaneously.[35–41] Inspired by PISA, we envision that the synthesis of well-defined CMs might also be realized by chemical synthesis and self-assembly in one-step, without the fabrication and purification of patchy colloidal building blocks. Using isotropic diblock copolymer spheres as seeds, the polymerization of third blocks produces attractive patches on spheres, which combine colloids into anisotropic CMs *in situ*. Therefore, CMs are achieved directly *via* seeded polymerization, without the preparation and purification of patchy intermediates. We address this strategy as polymerization-induced particle-assembly (PIPA).

Herein, we demonstrate a direct approach for the mass production of BCP CMs based on dispersion RAFT polymerization. We perform the polymerization using spherical seeds of poly(*N*,*N*-dimethylaminoethyl methacrylate)-*b*-poly(benzyl methacrylate) (PDMA-*b*-PBzMA). The polymerization of 2-hydroxypropyl methacrylate (HPMA) produces a linear PDMA-*b*-PBzMA-*b*-PHPMA triblock terpolymer. Thus, PHPMA domains function as attractive patches and connect colloid atoms (CAs) into AB_n-type CMs *in situ*. The stability of CMs is ensured by

[a]Key Laboratory of Organic Optoelectronics and Molecular Engineering, Department of Chemistry, Tsinghua University, Beijing 100084, China. E-mail: yuanjy@mail.tsinghua.edu.cn

[b]Department of Chemical Engineering, Tsinghua University, Beijing 100084, China. E-mail: yangzhenzhong@tsinghua.edu.cn

† This work is dedicated to Professor Caiyuan Pan, University of Science and Technology of China, for his 80th birthday in May, 2020.

‡ Electronic supplementary information (ESI) available: Experimental details and figures. See DOI: 10.1039/d0sc00219d

§ These authors contributed equally.

limiting conversions to *ca.* 50%, and the pH is ~ 2. Without post-purification, $PDMA_{70}$-*b*-$PBzMA_{96}$-*b*-$PHPMA_{70}$ yields 78.5% AB_2 CMs as prepared, in concentrated solution (50 g L^{-1}). The polymer-based AB_2-type CMs are intrinsically self-assembled, soft and programmable, offering the possibility to act as subunits for higher-level structures. We have realized the large-scale preparation of AB_n-type CMs *via* polymerization-induced self-assembly of spherical colloids, which is an efficient strategy achieving CMs and other hierarchical nanoparticles (HNPs) by synthesis and self-assembly in one step. This strategy can be readily applied to vastly different block copolymer systems, which would largely enrich the functional complexity of CMs and broaden their applications.

Results and discussion

Scheme 1 shows the synthesis of AB_2-type CMs by aqueous seeded RAFT polymerization. Spherical $PDMA_{70}$-*b*-$PBzMA_{96}$ seeds are produced by dispersion RAFT polymerization of BzMA in ethanol, using a PDMA macro-chain transfer agent. The $PDMA_{70}$-*b*-$PBzMA_{96}$ seeds are then transferred into water by dialysis, and a desired amount of aqueous HCl is added to adjust pH to ~ 2. The protonation of the PDMA stabilizer provided electrostatic repulsion for the stabilization of CMs.[42,43] The aqueous seeded polymerization of HPMA generated a $PDMA_{70}$-*b*-$PBzMA_{96}$-*b*-$PHPMA_{70}$ triblock terpolymer, which self-assembles hierarchically into AB_2-type CMs.

Fig. 1a shows the $PDMA_{70}$-*b*-$PBzMA_{96}$ spheres with a core diameter of 31 nm. The polymerization of HPMA produces a linear $PDMA_{70}$-*b*-$PBzMA_{96}$-*b*-$PHPMA_{70}$ triblock terpolymer ($Đ$ = 1.59), as studied by ^{1}H NMR and SEC (Fig. S3 and S4‡). A relatively high dispersity is due to the relatively low blocking efficiency caused by the embedding of CTA in PBzMA cores[44] and the crosslinking of PHPMA.[45] The growth of PHPMA blocks leads to the shift of particle size from 31 nm to 52 nm, indicating the formation of nanoparticle clusters (Fig. 1b). The cryo-TEM image (Fig. 1e) shows well-defined three-segment clusters (aka AB_2-CMs), resulting from seeded polymerization. We can find two dark grey CAs on each end as peripheral CAs, with the same size of $PDMA_{70}$-*b*-$PBzMA_{96}$ CAs (31 nm). The central CAs are much brighter in observation, suggesting a different chemical composition of middle CAs from cap CAs.

The composition of AB_2 CMs is further confirmed by TEM characterization of samples stained with RuO_4 and phosphotungstic acid (PTA), respectively. Fig. 1c shows that PDMA is located at the surface of peripheral CAs (PTA staining: PDMA black, PBzMA grey, and PHPMA not visible). And Fig. 1d reveals that satellite CAs are comprised of PBzMA (RuO_4 staining: PBzMA black, and PDMA and PHPMA not observable). Thus, we confirmed that central CAs were composed of newly formed PHPMA blocks. As described above, we have achieved $PDMA_{70}$-*b*-$PBzMA_{96}$-*b*-$PHPMA_{70}$ AB_2 CMs *in situ* during the polymerization, and the bonding angle of B-A-B is essentially 180° (Fig. S5‡), in analogy to the linear molecule of CO_2.

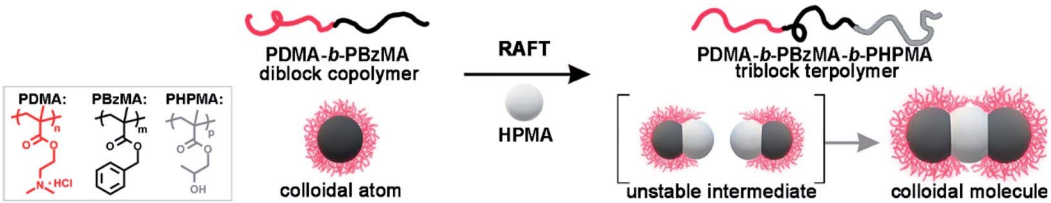

Scheme 1 The synthesis of AB_2-type CMs through polymerization-induced particle-assembly (PIPA).

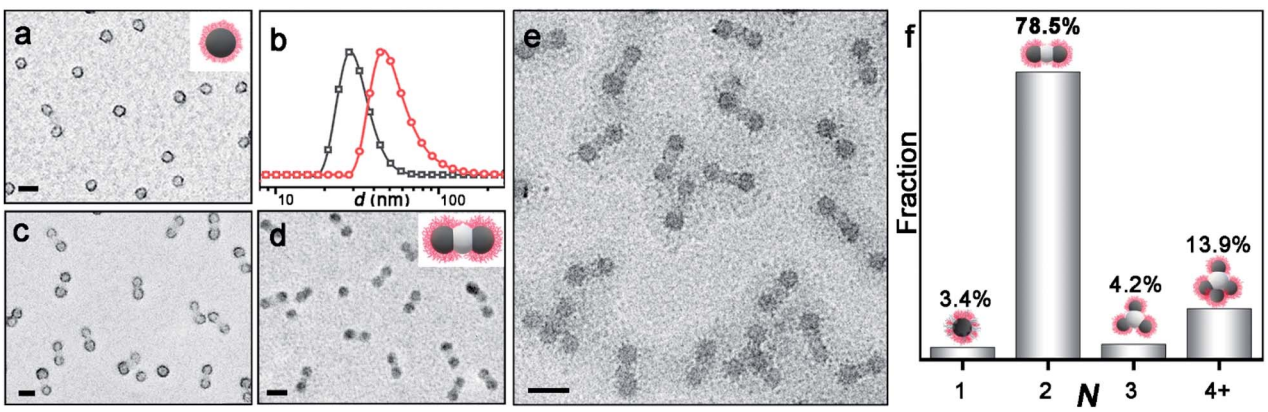

Fig. 1 (a) TEM image of $PDMA_{70}$-*b*-$PBzMA_{96}$ CAs after PTA-staining of the PDMA corona with the inset schematic structure. (b) DLS profiles of $PDMA_{70}$-*b*-$PBzMA_{96}$ CAs (black) and $PDMA_{70}$-*b*-$PBzMA_{96}$-*b*-$PHPMA_{70}$ CMs (red). (c and d) TEM image of $PDMA_{70}$-*b*-$PBzMA_{96}$-*b*-$PHPMA_{70}$ CMs after PTA-staining and RuO_4-staining, respectively; inset shows the schematic structure of AB_2-type CM. (e) Cryo-TEM image of CMs. (f) Distribution of AB_n-type CMs with varied valence numbers (N) obtained by statistically analysing 735 random particles by cryo-TEM. The valence number (N): 1, 2, 3, and 4+ correspond to AB_1, AB_2, AB_3, and AB_n ($n \geq 4$), respectively. All the scale bars are 50 nm.

Notably, $PDMA_{70}$-*b*-$PBzMA_{96}$-*b*-$PHPMA_{70}$ forms the major product of AB_2-type CMs (78.5%), with relative distribution shown in Fig. 1f. The sample was collected and analyzed as prepared, without multi-step purification. And the aqueous dispersion is more concentrated (50 g L^{-1}) than previously reported selective solvents (5 g L^{-1}).[25,46] The above experimental results demonstrate that this approach is robust and reliable for the mass preparation of AB_2-type CMs, which is especially beneficial for scalable applications.

The polymerization conditions for CM synthesis were optimized after kinetic study. Targeting $PDMA_{70}$-*b*-$PBzMA_{96}$-*b*-$PHPMA_{200}$ with a 10 wt% solid content, the polymerization reached 71.1% monomer conversion at 1.5 h (Fig. S7‡). And at 78.3% conversion (2 h), a mixture of AB_4 and large clusters was obtained. When the polymerization reached 90.7% conversion (4 h), large clusters were obtained possibly due to inter-cluster association and crosslinking between large PHPMA patches. To avoid clustering, we synthesize CM samples with the control of monomer conversion at *ca.* 50%.

A series of PDMA-*b*-PBzMA-*b*-PHPMA triblock terpolymer samples showed the morphology evolution of the AB_n-type CMs. $PDMA_{70}$-*b*-$PBzMA_{96}$-*b*-$PHPMA_{20}$ remains as symmetric spheres (Fig. 2a). This is understandable because PHPMA is too short to form visible domains by phase separation. For $PDMA_{70}$-*b*-$PBzMA_{96}$-*b*-$PHPMA_{46}$ with a longer PHPMA chain, 37.8% AB_2 CMs coexist with 58.3% spherical colloids (Fig. 2b). This is because, as the PHPMA domain exceed a critical size during continuing polymerization, the PDMA chains that stabilize the colloids are no longer able to cover them. As a result, the colloids become unstable due to largely increased surface energy (as will be discussed in detail later) and tend to bind together and form CMs to minimize the surface. Only a small number of Janus intermediates are captured in samples with a larger molecular weight (Fig. S6‡). Then AB_2 dominates $PDMA_{70}$-*b*-$PBzMA_{96}$-*b*-$PHPMA_{70}$ with a purity of 78.5% (Fig. 2c). Further growth of PHPMA leads to AB_n-type CMs with n larger than two. $PDMA_{70}$-*b*-$PBzMA_{96}$-*b*-$PHPMA_{109}$ generates a mixture of 50.2% AB_2, 15.7% AB_3, 22.9% AB_4 (Fig. 2d). The hydrodynamic diameter of clusters grows significantly with the growth of PHPMA (Fig. 2e).

The increasing DP of PHPMA leads to the increase of the PHPMA/PBzMA volume ratio (V_H/V_B), which plays a key role in determining the size and valence of CMs. Fig. 2f shows the distribution of valence shifts towards a higher value, as V_H/V_B increases. As V_H/V_B increases from 0.34 to 1.87, the number average of valence (N_n) gradually increases from 1 to 2.73 (Fig. 2g). For $PDMA_{70}$-*b*-$PBzMA_{96}$-*b*-$PHPMA_{70}$, the valence distribution is relatively narrow for a large-scale fabrication of CMs ($N_n = 2.31$, $Đ = 1.11$). Overall, we have generated a diversity of AB_n-type CMs with mean valence increasing with V_H/V_B.

When V_H/V_B reached 5.48 ($PDMA_{70}$-*b*-$PBzMA_{96}$-*b*-$PHPMA_{319}$), we have observed CMs of different valences (n = 3–6) with molecular precision (Fig. 3a), *i.e.* linear AB_2, triangular AB_3, tetrahedral AB_4, trigonal bipyramidal AB_5, square pyramidal AB_5 and octahedral AB_6, which are colloidal analogues of molecules like beryllium chloride ($BeCl_2$), boron trifluoride

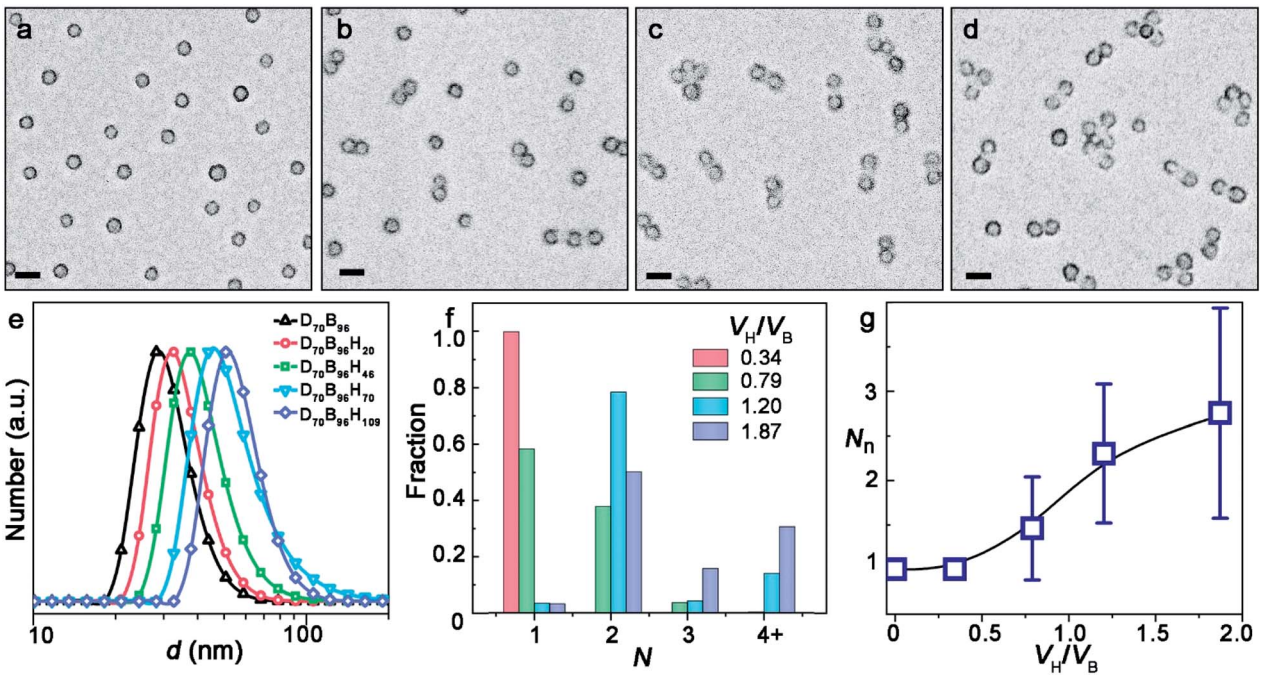

Fig. 2 (a–d) TEM images of $PDMA_{70}$-*b*-$PBzMA_{96}$-*b*-$PHPMA_z$ with varied z (20, 46, 70, and 109) after PTA-staining (PDMA black, PBzMA grey, and PHPMA invisible). Scale bars are 50 nm. (e) DLS profiles of the colloid samples. $PDMA_{70}$-*b*-$PBzMA_{96}$-*b*-$PHPMA_z$ is abbreviated to $D_{70}B_{96}H_z$. (f) Distribution of CMs with varied valence numbers (N) determined by statistically analyzing the TEM images with the inset V_H/V_B ratios. (g) Number average valence (N_n) of $PDMA_{70}$-*b*-$PBzMA_{96}$-*b*-$PHPMA_z$ CMs against V_H/V_B. Error bars represent standard deviation. $N_n = \sum_{i=1}^{m} n_i N_i \Big/ \sum_{i=1}^{m} N_i$, $N_w = \sum_{i=1}^{m} n_i N_i^2 \Big/ \sum_{i=1}^{m} n_i N_i$, $Đ = N_w/N_n$.

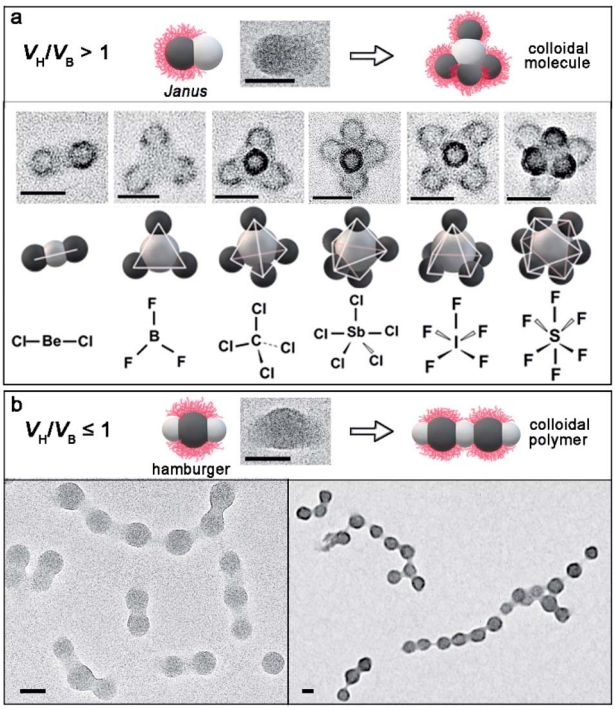

Fig. 3 (a) Self-assembly of the $PDMA_{70}$-*b*-$PBzMA_{96}$-*b*-$PHPMA_{319}$ triblock terpolymer toward CMs with $V_H/V_B > 1$; inset shows the cryo-TEM image of the unstable Janus intermediate. TEM images of varied PDMA-*b*-PBzMA-*b*-PHPMA CMs after PTA-staining; inset shows schematic structures and molecules. (b) Illustrative self-assembly of PDMA-*b*-PBzMA-*b*-PHPMA at $V_H/V_B \leq 1$. Cryo-TEM (bottom, left) and TEM images (bottom, right) after PTA-staining of $PDMA_{70}$-*b*-$PBzMA_{321}$-*b*-$PHPMA_{169}$ colloidal chains *via* the "Hamburger" (insert) structure. Scale bars are 50 nm.

(BF_3), carbon tetrachloride (CCl_4), antimonic chloride ($SbCl_5$), iodine pentafluoride (IF_5) and sulfur hexafluoride (SF_6), respectively. In contrast, using larger CAs targeting $V_H/V_B \leq 1$, linear colloidal polymers ($PDMA_{70}$-*b*-$PBzMA_{321}$-*b*-$PHPMA_{169}$) are obtained, by the polymerization of "hamburger" intermediates (Fig. 3b).

We therefore propose the formation mechanism of AB_n-type CMs by polymerization-induced particle-assembly (PIPA): (1) PDMA-*b*-PBzMA forms spherical core–shell CAs with PBzMA blocks as rubbery cores ($T_g = 56.8$ °C),[47] and PDMA chains as soluble stabilizers locating on the surface. (2) The polymerization produces PHPMA blocks which phase separate with PBzMA blocks, and aggregate into PHPMA micro-domains. (3) When the attractive PHPMA domains reach a critical size, they combine into PHPMA central CAs and unify PDMA-*b*-PBzMA spheres into colloidal clusters. (4) The structure of colloidal clusters is determined by V_H/V_B. When $V_H/V_B > 1$, the assembly of unstable monovalent Janus intermediates produces AB_n-type CMs, with n regulated by V_H/V_B. When $V_H/V_B \leq 1$, divalent hamburger-shape intermediates form colloidal chains.

This is in agreement with the principle of solvent-based fabrication of multicompartment micelles (MCMs), reported by Müller and coworkers.[25,26] They have systematically studied the self-assembly of an ABC triblock terpolymer system (A as the attractive corona, B as the core, and C as the repulsive corona). The strong phase separation between A and B generates a patchy structure based on V_A/V_B. $V_A/V_B > 1$ yields monovalent Janus intermediates, with one attractive A patch and one repulsive C patch, which generate cluster-like MCMs. Oppositely, $V_A/V_B \leq 1$ leads to divalent "hamburger" subunits with two attractive A patches and one repulsive C patch, which then assemble into chain-like MCMs. This concept has been validated by vastly different linear triblock terpolymer systems for the fabrication of both spherical MCMs and linear MCMs.

The formation of AB_n-like CMs requires PHPMA domains protruding from PBzMA cores, not growing inside PBzMA cores. The interfacial energy is the critical parameter determining the CM formation during polymerization. Compared to the entropy cost of stretching chains, and the repulsive interactions among stabilizer chains, interfacial energies are dominant in the formation of AB_n-type CMs. After neglecting free energies contributed by core-stretching and corona repulsion, the whole free energy change is written as

$$\Delta F = \sum_i \gamma_i A_i$$

γ_i and A_i: interfacial tension and area of the i^{th} interface. For an ABC linear triblock terpolymer with A as the stabilizer, B phase separates with C. when the interfacial tension between B cores and solution (γ_{B-S}) is higher than that between C cores and solution (γ_{C-S}) ($\gamma_{B-S} > \gamma_{C-S}$), the C block tends to aggregate at the B/solvent interface. As a result, the C block forms micro-domains serving as attractive patches. Otherwise, C micro-domains might aggregate inside the B cores, and raspberry-like MCMs are possibly obtained as Armes and coworkers have reported.[48–50] As shown in Table S5,‡ the interfacial tensions were measured by the Owens–Wendt–Rabel–Kaelble method.[51,52] The interfacial tensions of PHPMA–water (γ_{H-W}) and PBzMA–water (γ_{B-W}) interfaces are 9.0 ± 1.6 mN m^{-1} and 27.1 ± 2.5 mN m^{-1}, respectively. Since $\gamma_{H-W} < \gamma_{B-W}$, the PHPMA blocks aggregate at the PBzMA/water interfaces. Therefore, CMs are favored compared to raspberry-like MCMs (Scheme 2).

The PIPA strategy is an extension of PISA for the rational design and mass production of BCP nanoparticles with structural hierarchies. The design of the ABC triblock terpolymer requires (1) strong phase separation between B and C blocks and (2) monomer C suitable for PISA. And the morphology of HNPs is tuned by the interfacial tension and the V_C/V_B of the ABC triblock terpolymer. Based on these requirements, PIPA could be applied to vastly different triblock systems. For example, we also studied the aqueous seeded polymerization of diacetone acrylamide (DAAm), using $PDMA_{70}$-*b*-$PBzMA_{96}$ spheres as seeds. $PDMA_{70}$-*b*-$PBzMA_{96}$-*b*-$PDAAm_{95}$ ($Đ = 1.38$) assembled into a mixture of AB_2 and AB_4 CMs (Fig. S21‡), with PDAAm as an attractive domain. As the DP of PDAAm increased, $PDMA_{70}$-*b*-$PBzMA_{96}$-*b*-$PDAAm_{114}$ ($Đ = 1.52$) produced majorly AB_4 CMs (Fig. S22‡). Our strategy could be readily applied to different triblock terpolymer systems for the fabrication of HNPs with different hierarchies and functionalities. Moreover, the discussed considerations of directing the process may well serve as an inspiration for other hierarchical self-assembly systems.

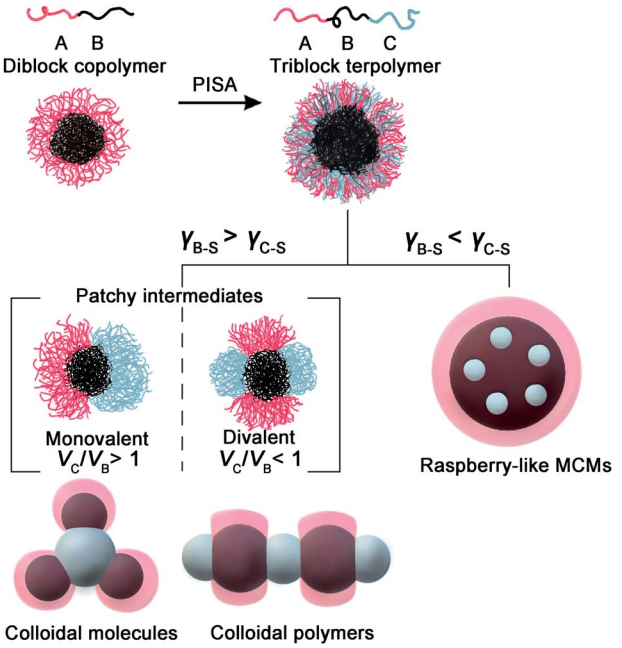

Scheme 2 Illustrations of PIPA targeting colloidal molecules, colloidal polymers, and raspberry-like MCMs, respectively, by tuning the interfacial tensions (γ_{B-S} and γ_{C-S}) and the volume ratio (V_C/V_B).

Conclusions

In summary, we have developed a straightforward way to fabricate BCP AB_n-type CMs by seeded polymerization. A variety of well-defined CMs have been fabricated, including linear AB_2, triangular AB_3, tetrahedral AB_4, trigonal bipyramidal AB_5, square pyramidal AB_5 and octahedral AB_6. At a low volume ratio, colloidal chains were achieved by assembly of "hamburger" intermediates. Polymerization-induced particle-assembly allows the large scale production of the CMs, *e.g.* AB_2-CMs (78.5% purity, more than 10^{17} particles, 50 g L^{-1}). The CMs can serve as new building blocks for more complex structures such as colloidal chains and colloidal networks. The PIPA approach could be readily applied to vastly different triblock terpolymer systems for the fabrication of functional HNPs and has unique advantages for further applications.

Conflicts of interest

There are no conflicts to declare.

Acknowledgements

We thank Danyang Li and Xiaofeng Hu at the National Center for Protein Science (Beijing) Tsinghua Cryo-EM Facility for the technical support, and Prof. Xiaosong Wang at the University of Waterloo for helpful discussion. This work was supported by the National Natural Science Foundation of China (21871162 and 51573086).

Notes and references

1 Q. Chen, J. K. Whitmer, S. Jiang, S. C. Bae, E. Luijten and S. Granick, *Science*, 2011, **331**, 199–202.
2 C. Zeng, Y. Chen, K. Kirschbaum, K. J. Lambright and R. Jin, *Science*, 2016, **354**, 1580–1584.
3 P.-E. Rouet, C. Chomette, E. Duguet and S. Ravaine, *Angew. Chem., Int. Ed.*, 2018, **57**, 15754–15757.
4 Z. Wang, Z. Wang, J. Li, S. T. H. Cheung, C. Tian, S.-H. Kim, G.-R. Yi, E. Ducrot and Y. Wang, *J. Am. Chem. Soc.*, 2019, **141**, 14853–14863.
5 D. J. Lunn, J. R. Finnegan and I. Manners, *Chem. Sci.*, 2015, **6**, 3663–3673.
6 L. Yang, L. Meng, J. Song, Y. Xiao, R. Wang, H. Kang and D. Han, *Chem. Sci.*, 2019, **10**, 7466–7471.
7 K. Miszta, J. de Graaf, G. Bertoni, D. Dorfs, R. Brescia, S. Marras, L. Ceseracciu, R. Cingolani, R. van Roij, M. Dijkstra and L. Manna, *Nat. Mater.*, 2011, **10**, 872–876.
8 Z. Yang, J. Wei, Y. I. Sobolev and B. A. Grzybowski, *Nature*, 2018, **553**, 313–318.
9 A. Walther and A. H. E. Müller, *Chem. Rev.*, 2013, **113**, 5194–5261.
10 Q. Yan, J. Yuan, Z. Cai, Y. Xin, Y. Kang and Y. Yin, *J. Am. Chem. Soc.*, 2010, **132**, 9268–9270.
11 R. Schreiber, J. Do, E.-M. Roller, T. Zhang, V. J. Schüller, P. C. Nickels, J. Feldmann and T. Liedl, *Nat. Nanotechnol.*, 2013, **9**, 74–78.
12 B. Ruzicka, E. Zaccarelli, L. Zulian, R. Angelini, M. Sztucki, A. Moussaïd, T. Narayanan and F. Sciortino, *Nat. Mater.*, 2010, **10**, 56–60.
13 W. Liu, M. Tagawa, H. L. Xin, T. Wang, H. Emamy, H. Li, K. G. Yager, F. W. Starr, A. V. Tkachenko and O. Gang, *Science*, 2016, **351**, 582–586.
14 Z. Huang, J. Gong and Z. Nie, *Acc. Chem. Res.*, 2019, **52**, 1125–1133.
15 F. Li, D. P. Josephson and A. Stein, *Angew. Chem., Int. Ed.*, 2011, **50**, 360–388.
16 E. Duguet, A. Désert, A. Perro and S. Ravaine, *Chem. Soc. Rev.*, 2011, **40**, 941–960.
17 L. Yao, Q. Li, Y. Guan, X. X. Zhu and Y. Zhang, *ACS Macro Lett.*, 2018, **7**, 80–84.
18 A. Perro, E. Duguet, O. Lambert, J.-C. Taveau, E. Bourgeat-Lami and S. Ravaine, *Angew. Chem., Int. Ed.*, 2009, **48**, 361–365.
19 N. B. Schade, M. C. Holmes-Cerfon, E. R. Chen, D. Aronzon, J. W. Collins, J. A. Fan, F. Capasso and V. N. Manoharan, *Phys. Rev. Lett.*, 2013, **110**, 148303.
20 C. Yi, Y. Yang and Z. Nie, *J. Am. Chem. Soc.*, 2019, **141**, 7917–7925.
21 Z. Gong, T. Hueckel, G.-R. Yi and S. Sacanna, *Nature*, 2017, **550**, 234–238.
22 Y. Tian, T. Wang, W. Liu, H. L. Xin, H. Li, Y. Ke, W. M. Shih and O. Gang, *Nat. Nanotechnol.*, 2015, **10**, 637–644.
23 M. Y. Ben Zion, X. He, C. C. Maass, R. Sha, N. C. Seeman and P. M. Chaikin, *Science*, 2017, **358**, 633–636.

24 W. Ren, S. Wen, S. A. Tawfik, Q. P. Su, G. Lin, L. A. Ju, M. J. Ford, H. Ghodke, A. M. van Oijen and D. Jin, *Chem. Sci.*, 2018, **9**, 4352–4358.
25 A. H. Gröschel, F. H. Schacher, H. Schmalz, O. V. Borisov, E. B. Zhulina, A. Walther and A. H. E. Müller, *Nat. Commun.*, 2012, **3**, 710.
26 A. H. Gröschel, A. Walther, T. I. Löbling, F. H. Schacher, H. Schmalz and A. H. E. Müller, *Nature*, 2013, **503**, 247.
27 Z. Zhang, C. Zhou, H. Dong and D. Chen, *Angew. Chem., Int. Ed.*, 2016, **55**, 6182–6186.
28 Z. Zhang, H. Li, X. Huang and D. Chen, *ACS Macro Lett.*, 2017, **6**, 580–585.
29 R. Deng, H. Li, F. Liang, J. Zhu, B. Li, X. Xie and Z. Yang, *Macromolecules*, 2015, **48**, 5855–5860.
30 É. Ducrot, M. He, G.-R. Yi and D. J. Pine, *Nat. Mater.*, 2017, **16**, 652–657.
31 J. S. Oh, S. Lee, S. C. Glotzer, G.-R. Yi and D. J. Pine, *Nat. Commun.*, 2019, **10**, 3936.
32 Y. Mai and A. Eisenberg, *Chem. Soc. Rev.*, 2012, **41**, 5969–5985.
33 X. Wang, G. Guerin, H. Wang, Y. Wang, I. Manners and M. A. Winnik, *Science*, 2007, **317**, 644.
34 H. Sun, D. Liu and J. Du, *Chem. Sci.*, 2019, **10**, 657–664.
35 X. Chen, L. Liu, M. Huo, M. Zeng, L. Peng, A. Feng, X. Wang and J. Yuan, *Angew. Chem., Int. Ed.*, 2017, **56**, 16541–16545.
36 X.-F. Xu, C.-Y. Pan, W.-J. Zhang and C.-Y. Hong, *Macromolecules*, 2019, **52**, 1965–1975.
37 J. C. Foster, S. Varlas, B. Couturaud, Z. Coe and R. K. O'Reilly, *J. Am. Chem. Soc.*, 2019, **141**, 2742–2753.
38 P. Yang, Y. Ning, T. J. Neal, E. R. Jones, B. R. Parker and S. P. Armes, *Chem. Sci.*, 2019, **10**, 4200–4208.
39 X. Wang, S. Man, J. Zheng and Z. An, *ACS Macro Lett.*, 2018, **7**, 1461–1467.
40 S. Guan, Z. Deng, T. Huang, W. Wen, Y. Zhao and A. Chen, *ACS Macro Lett.*, 2019, **8**, 460–465.
41 S. Li, H. Nie, S. Gu, Z. Han, G. Han and W. Zhang, *ACS Macro Lett.*, 2019, **8**, 783–788.
42 M. Williams, N. J. W. Penfold and S. P. Armes, *Polym. Chem.*, 2016, **7**, 384–393.
43 D. Zhou, S. Dong, R. P. Kuchel, S. Perrier and P. B. Zetterlund, *Polym. Chem.*, 2017, **8**, 3082–3089.
44 Y. Zhang, L. Yu, X. Dai, L. Zhang and J. Tan, *ACS Macro Lett.*, 2019, **8**, 1102–1109.
45 A. Blanazs, J. Madsen, G. Battaglia, A. J. Ryan and S. P. Armes, *J. Am. Chem. Soc.*, 2011, **133**, 16581–16587.
46 A. H. Gröschel, A. Walther, T. I. Löbling, J. Schmelz, A. Hanisch, H. Schmalz and A. H. E. Müller, *J. Am. Chem. Soc.*, 2012, **134**, 13850–13860.
47 M. Huo, M. Zeng, D. Li, L. Liu, Y. Wei and J. Yuan, *Macromolecules*, 2017, **50**, 8212–8220.
48 F. S. Bates, *Science*, 1991, **251**, 898–905.
49 P. Chambon, A. Blanazs, G. Battaglia and S. P. Armes, *Macromolecules*, 2012, **45**, 5081–5090.
50 W. Kong, W. Jiang, Y. Zhu and B. Li, *Langmuir*, 2012, **28**, 11714–11724.
51 D. K. Owens and R. C. Wendt, *J. Appl. Polym. Sci.*, 1969, **13**, 1741–1747.
52 D. H. Kaelble, *J. Adhes.*, 1970, **2**, 66–81.

